AJNR

MR Imaging of Intracranial Fluid Levels

James J. Abrahams, Mika Lidov and Carlos Artiles

MR Imaging of Intracranial Fluid Levels

James J. Abrahams[1]
Mika Lidov
Carlos Artiles

Six patients with seven intracranial fluid levels were evaluated with both CT and MR at 1.5 T. A surgical diagnosis was obtained in six of the seven instances. MR was found to be superior to CT in detecting intracranial fluid levels, and the MR signal characteristics were helpful in identifying their contents. These cases demonstrate the necessity for a slightly different approach to lesions with fluid levels. In one patient, imaging in the prone position allowed detection of a solid component; in several others, detection of the fluid level was dependent on the selection of nonroutine windows and levels. Fluid levels are classified with respect to their components and MR features.

MR is superior to CT in imaging fluid levels. The appearance of fluid levels on MR varies with their composition, the ratio of the components, the sequence parameters, and the position of the patient.

Some intracranial lesions that have a cystic appearance on MR and CT are later demonstrated at surgery to be solid. A fluid level is the only preoperative radiographic finding that unequivocally proves a lesion is cystic. The impact this finding can have on the differential diagnosis and the surgical technique is obvious. We describe the MR characteristics of fluid levels in a variety of intracranial lesions and demonstrate the superior ability of MR in comparison with CT in detecting and characterizing them. The fluid levels are categorized according to their components, and the MR features of the three most common kinds (air-fluid, fluid-precipitate, and fat-fluid) are discussed.

Materials and Methods

Six patients with seven intracranial fluid levels were evaluated by MR, and the findings were compared with those on CT (Table 1). A surgical diagnosis was obtained in six of the seven instances. Patients who did not have both a CT and MR scan were excluded from the study. The study included five males and one female 10–72 years old.

A high-field-strength (1.5-T) superconducting MR scanner was used.* T1-weighted, 400, 600/20 (TR/TE), and T2-weighted multiecho, 2000, 2500/20, 80, sequences were acquired. The width and level were adjusted for maximum visualization of the fluid levels. One patient (case 1) was scanned in both the supine and prone positions.

CT scans were obtained 1 day before the MR scans in cases 5 and 6 and 2 and 3 days before the MR scans in cases 1 and 3, respectively. In case 2, sequential CT scans were obtained, with the last CT scan being obtained 2½ months prior to MR. In case 4, a CT scan was obtained 3 weeks after the MR scan.

Case Reports

Case 1

A 42-year-old man was seen with recent onset of slowly progressive cranial-nerve deficits. A CT scan demonstrated questionable areas of low and high attenuation in the left pons without evidence of a fluid level (Fig. 1A). MR, initially performed on a low-field-strength (0.15-

* General Electric, Milwaukee, WI.

ABRAHAMS ET AL.

TABLE 1: Summary of Patients with Intracranial Fluid Levels Evaluated by CT and MR

Classification/ Case No.	Pathology	Detection of Fluid Level	
		CT	MR
Fluid-precipitate			
1	Vascular malformation with hemorrhagic cyst	Not seen	T1: seen well after width & level adjustment T2: seen well
2	Arachnoid cyst resection with hemorrhagic surgical bed	Not seen initially[a]	T1: seen poorly after width & level adjustment T2: seen well after width & level adjustment
3	Cystic schwannoma of hypoglossal nerve	Not seen initially[a]	T1 & T2: seen well
4	Chromophobe adenoma with hemorrhagic cyst	Not seen	T1 & T2: seen well
5	Recurrent craniopharyngioma with hemorrhagic cyst	Not seen	T1: seen well after width & level adjustment T2: seen well
6	Intraventricular blood	Seen well	T1 & T2: seen well
Air-fluid			
6[b]	Intraventricular epithelial cyst	Seen well	T1: seen well after width & level adjustment T2: seen well

[a] After the fluid level was seen on MR, retrospective review of CT showed subtle findings suggesting a fluid level.
[b] This patient had two fluid levels.

T) scanner, showed a smooth, round, homogeneous high-signal pontine mass, but did not show a fluid level. A subsequent high-field-strength MR scan, however, clearly revealed a fluid level on the T2-weighted sequence, with a lower-signal-intensity component in the dependent position and a heterogeneous high-signal component in the nondependent layer (Figs. 1B, 1C, and 1E).

The complexity of the nondependent high-signal portion of the lesion suggested the possibility of a solid nodule. A repeat examination, performed with the patient in the prone position (Fig. 1D), readily revealed a fixed solid nodule that did not shift position while the fluid layers did.

The precise MR localization of the solid component of the lesion and the demonstration of its cystic nature changed what was believed to be an inoperable lesion into an operable one.

At surgery, a cystic lesion was entered, and a small arteriovenous malformation with adherent clot was excised. This clot corresponded exactly to the location of the nodule seen on the MR scan. Six months later the patient had resumed work and was playing tennis again.

Case 2

A 60-year-old woman had a left parietal arachnoid cyst resected at another hospital; the postoperative CT scan revealed a hemorrhagic surgical bed. Sequential CT scans over the next month showed resolution of the hemorrhage. At our institution, a fluid level, which was not initially appreciated on CT, was clearly demonstrated on MR (Fig. 2B). Retrospective review of the CT scan suggested a fluid level (Fig. 2A).

Case 3

A 59-year-old man was seen for MR evaluation of a complex posterior fossa lesion that was demonstrated on CT. No cystic component or fluid level was initially appreciated on CT (Fig. 3A). The MR scan that followed, however, beautifully demonstrated a large cystic area with a fluid level (Figs. 3B and 3C). The surgical approach was greatly facilitated by the ability of MR to differentiate the cystic from solid portions of the lesion.

At surgery, the cystic component contained a viscous yellow fluid. No blood was seen in the cyst and no hemosiderin was demonstrated histologically. The pathologic diagnosis was a cystic schwannoma.

Case 4

A 72-year-old man followed by ear, nose, and throat specialists for chronic vertigo and tinnitus had an MR scan of the internal auditory canal that revealed an incidental pituitary lesion with a fluid level composed of a very hypointense dependent layer and a hyperintense nondependent layer on the T2-weighted sequence (Fig. 4A). A subsequent CT scan failed to demonstrate this fluid level (Fig. 4B). Further questioning elicited two recent episodes of severe headache and nausea, which were believed to be consistent with pituitary apoplexy. The patient underwent transsphenoidal surgery, and a cyst containing subacute blood was encountered within the lesion. The pathologic diagnosis was chromophobe adenoma.

Case 5

A 10-year-old boy who had undergone debulking of a craniopharyngioma when he was 4 years old presented with signs and symptoms of hydrocephalus. CT and MR scans 1 day apart revealed recurrent tumor and hydrocephalus (Fig. 5). A fluid level was once again identified within the lesion on MR but not on CT. The dependent layer was hyperintense relative to brain on T1 images and markedly hypointense on T2 images, while the nondependent layer was very hyperintense on both T1- and T2-weighted images. It was believed from CT and MR that these findings represented hemorrhage with recurrent tumor, but the patient refused surgery.

Case 6

A 52-year-old man had a 1½-year history of right-sided headaches that occasionally were positional in nature. His neurologic examination was unremarkable. CT and MR scans demonstrated a cyst in the trigone of the right lateral ventricle (Fig. 6A). An attempt at rupturing
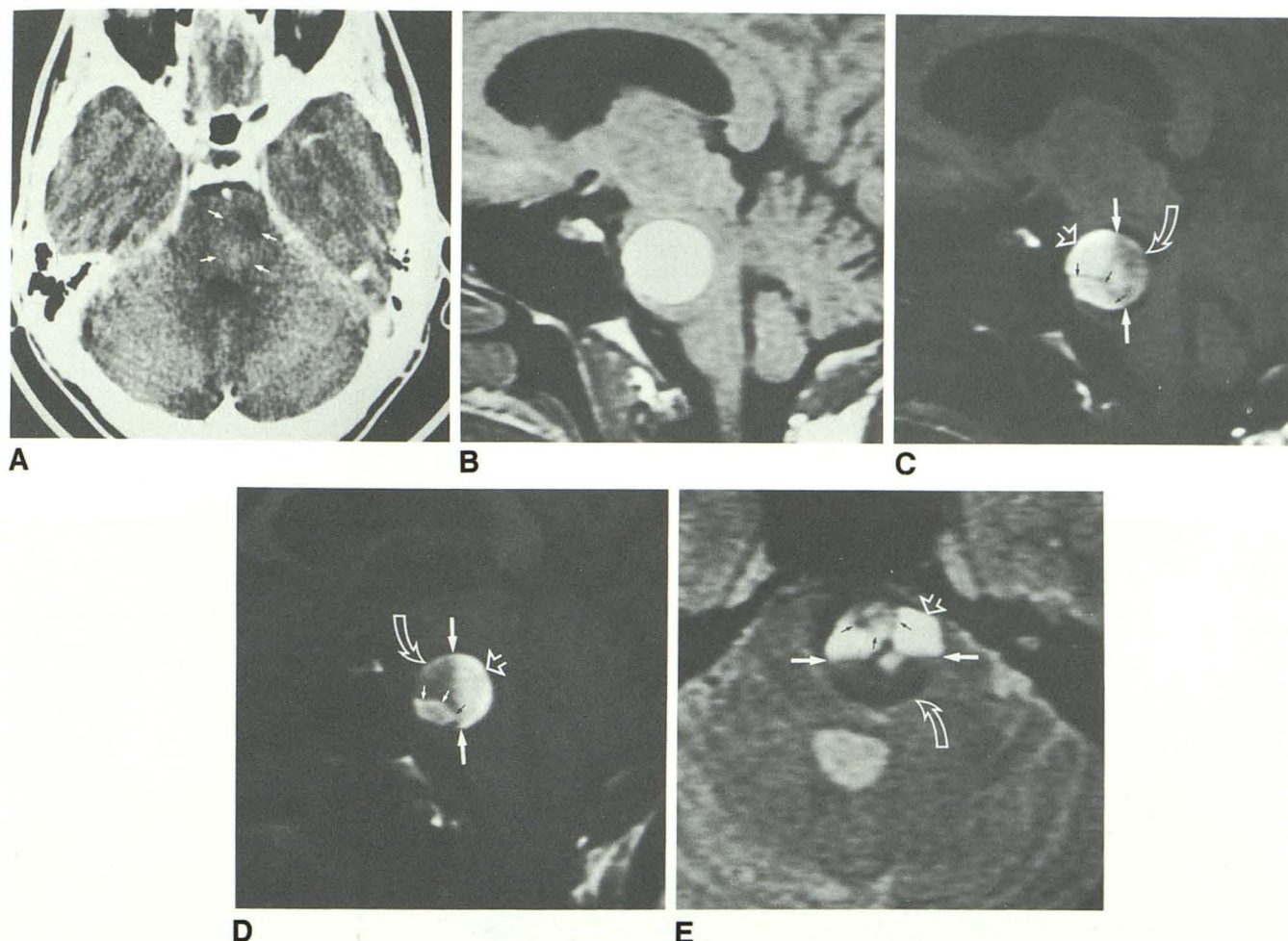
A   B   C

D   E

Fig. 1.—Case 1: Vascular malformation with a hemorrhagic cyst.

A, Axial contrast-enhanced CT scan. Areas of low and high attenuation (*arrows*) suggest a lesion in this location. No fluid level is seen.

B, Sagittal T1-weighted image (600/20) shows high-signal lesion in pons.

C, With width and level adjusted to allow visualization of fluid level (compare with *B*). High-signal free methemoglobin layer is in nondependent position (*straight open arrow*), while lower-signal intracellular deoxyhemoglobin and/or intracellular methemoglobin layer assume dependent position (*curved arrow*). Fluid level (*solid white arrows*). Nodule (*black arrows*).

D, Sagittal T1-weighted image (400/20) with patient in prone position. This causes fluid layers to swap positions while high-signal nodule (*small straight solid arrows*) remains fixed. Nodule is now better visualized against relatively lower-signal layer (*curved arrow*). (Compare with *C*.) Free methemoglobin (*straight open arrow*); fluid level (*long straight solid arrows*).

E, Axial T2-weighted image (2500/80). Low-signal intracellular deoxyhemoglobin and/or intracellular methemoglobin layer (*curved arrow*) have dropped further in signal intensity on this T2-weighted image. (Compare with *C*.) Nodule (*black arrows*); free methemoglobin (*straight open arrow*); fluid level (*solid white arrows*).

the cyst was made by passing a needle through a burr hole under sonographic guidance. Only partial decompression of the cyst was achieved. His symptoms resolved transiently, but recurred 4 months later. A CT and MR scan at that time showed that the cyst had enlarged. Therefore, the patient underwent surgical deroofing of the cyst. This lesion was diagnosed as an epithelial cyst at pathology and the patient did well postoperatively. The anterior portion of the cyst wall, which was left intact, allowed the formation of an air-fluid level, which was seen on postoperative CT and MR scans (Figs. 6B–6D). The nondependent air produced a signal void on all pulse sequences, while the dependent CSF layer behaved like CSF on all pulse sequences.

In addition to the air-fluid level demonstrated on the postoperative CT and MR scans, a blood-CSF level formed in the occipital horn of the lateral ventricle (Figs. 6E–6G). The fluid level was composed of a dependent layer that was slightly hypointense relative to brain on T1-weighted images and markedly hypointense on T2 images, and of a nondependent layer that behaved like CSF (Figs. 6F and 6G). On CT, the dependent layer was highly attenuating and the nondependent layer again behaved like CSF (Fig. 6E).

Results

MR was superior to CT in imaging fluid levels (Table 1). In cases 1–5, the fluid levels were readily seen on MR, but not on CT. In case 6, the fluid levels were seen equally well on MR and CT. Retrospective review of the CT scans did show subtle findings suggesting fluid levels in cases 2 and 3 (Figs. 2A and 3A), but these were not appreciated initially.
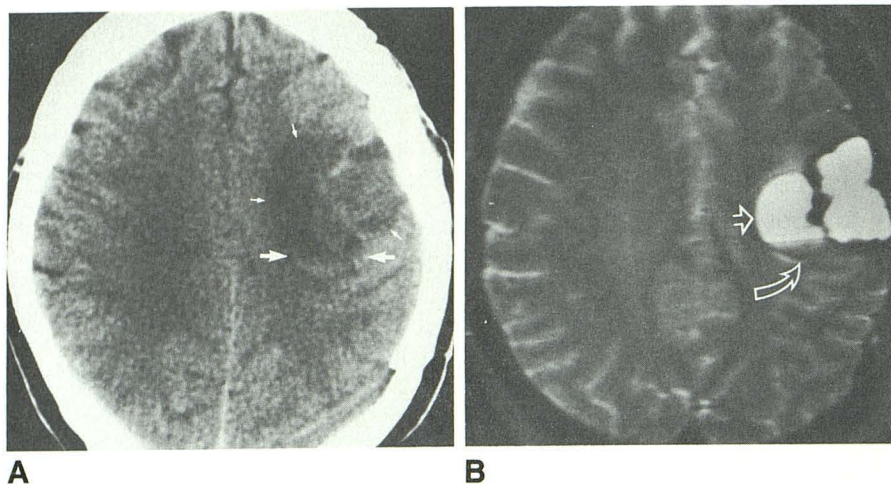
A

B

Fig. 2.—Case 2: Hemorrhagic surgical bed after resection of arachnoid cyst.

A, Axial CT scan. Retrospective review revealed findings suggestive of fluid level (*large arrows*). Lesion (*small arrows*).

B, Axial T2-weighted image (2500/80) clearly shows fluid level. High-signal free methemoglobin assumes nondependent position (*straight arrow*). Intracellular deoxyhemoglobin and/or intracellular methemoglobin (*curved arrow*).
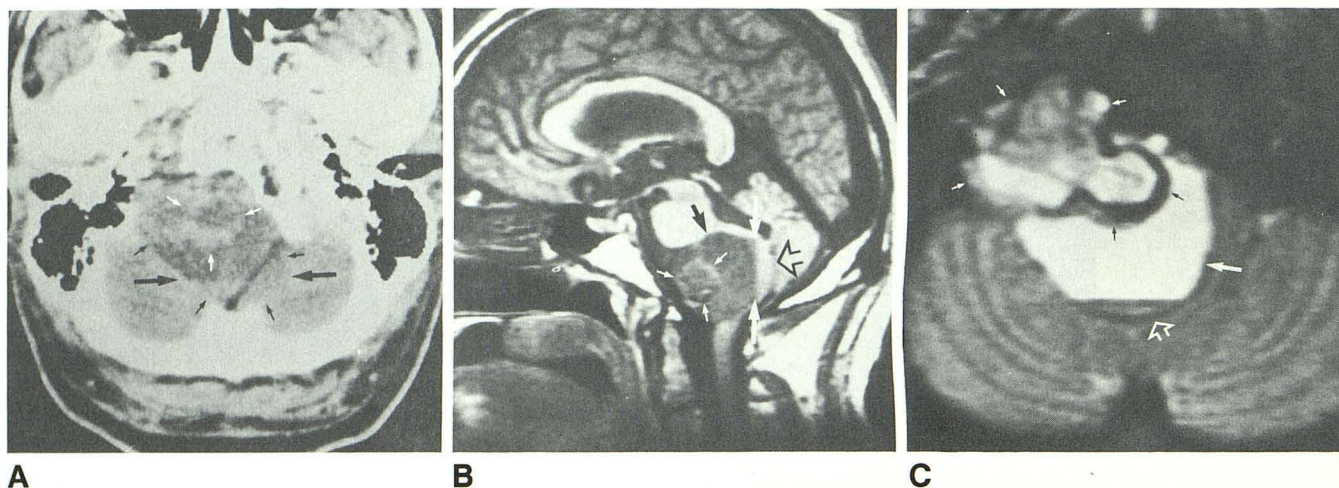

A

B

C

Fig. 3.—Case 3: Cystic schwannomas of hypoglossal nerve. Fluid level comprising proteinaceous cyst fluid and necrotic debris is evident.

A, Axial CT scan shows complex posterior fossa mass. Retrospective review revealed findings suggestive of fluid level (*large black arrows*). Solid component of lesion (*white arrows*); cystic component (*small black arrows*).

B, Sagittal T1-weighted image (600/20). Nondependent proteinaceous fluid layer (*solid black arrow*) has a slightly higher signal intensity than CSF in ventricles and cisterns. Dependent layer is presumed to be composed of necrotic debris (*open arrow*). Solid portion of lesion (*small white arrows*); fluid level (*large white arrows*).

C, Axial T2-weighted image (2500/80). Proteinaceous fluid has slightly higher signal than CSF (*large solid white arrow*), while necrotic debris is isointense relative to brain (*open arrow*). Solid portion of lesion (*solid arrows*).
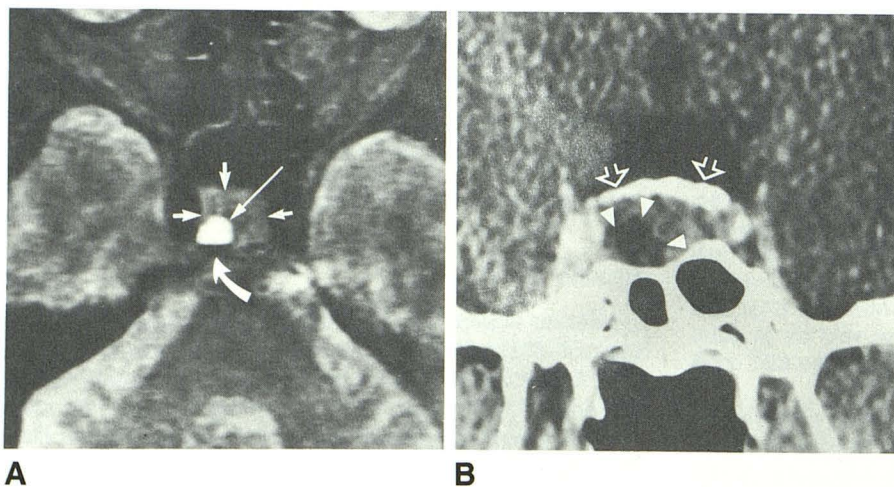

A

B

Fig. 4.—Case 4: Chromophobe adenoma with hemorrhagic cyst.

A, Axial T2-weighted MR image (2000/80). Fluid level is noted within lesion. Chromophobe adenoma (*short straight arrows*). Free methemoglobin layer (*long straight arrow*). Intracellular deoxyhemoglobin and/or intracellular methemoglobin (*curved arrow*).

B, Coronal CT scan through posterior sella turcica shows chromophobe adenoma with low-attenuating hemorrhagic cyst (*arrowheads*). Dorsum sellae (*arrows*).
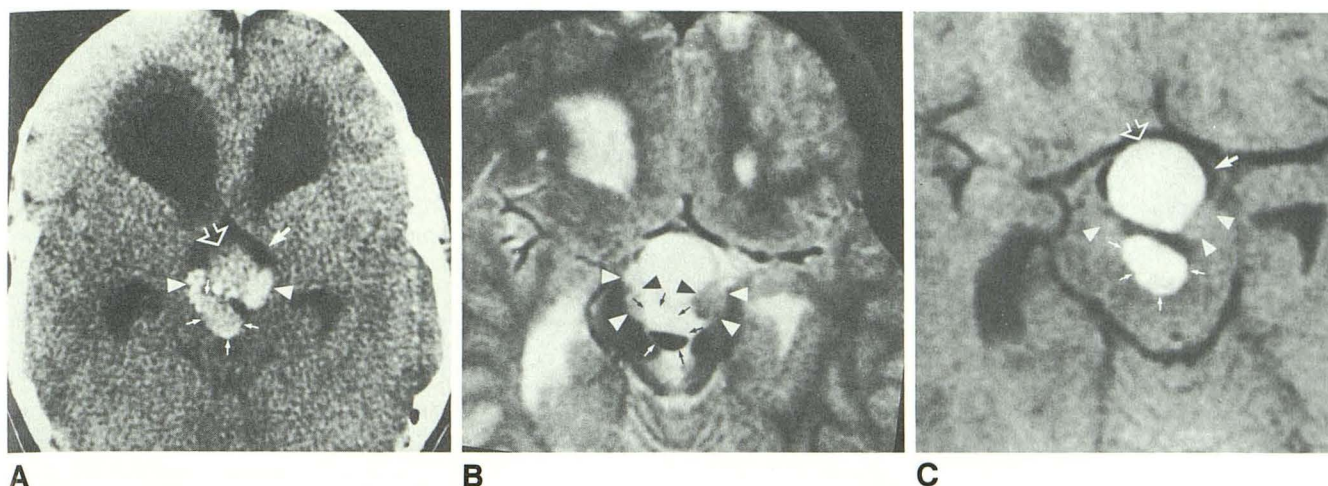
A   B   C

Fig. 5.—Case 5: Recurrent craniopharyngioma with fluid level.

A, Axial CT scan. Posterior cystic component (*small solid arrows*). Fluid level is not seen. Solid calcified portions of craniopharyngioma are seen (*arrowheads*). Anterior hemorrhagic component, without fluid level (*open arrow*). Third ventricle (*large solid arrow*).

B, Axial T2-weighted MR image (2000/80) corresponding to *A*. Two solid, calcified portions of lesion are noted (*arrowheads*). (Compare with *A*.) Within posterior cystic portion (*arrows*), fluid layer is seen. High-signal free methemoglobin layer assumes nondependent position.

C, Axial T1-weighted MR image (600/20) through circle of Willis. Note that when width and level are adjusted for brain parenchyma, as in this image, fluid level is not seen clearly. Solid portions of lesion (*arrowheads*); cystic portion (*small solid arrows*). Third ventricle invaginated by tumor (*large solid arrow*). Large, round, high-signal area (*open arrow*) in upper portion of lesion was also believed to be hemorrhagic focus, because it had high attenuation on concurrent CT scan (*A*) and low attenuation on previous CT scan. No fluid level was seen in this portion.

The MR signal characteristics of the fluid levels were helpful in identifying their contents in all cases. In addition, several other observations were made. It was found that adjusting the width and level was necessary, in some sequences, for visualization of the fluid levels (Table 1). When the level and width were adjusted for normal brain imaging, the fluid levels were not initially visualized on the T1 sequences in cases 1, 2, and 5 (Figs. 1B, 1C, and 5C) or on the T2 sequence in case 2. The air-CSF level in case 6 was seen with difficulty on the T1-weighted sequence (Fig. 6D). Changing the width and level, however, enabled us to detect these fluid levels readily. This point deserves special emphasis since widths and levels are routinely selected by technologists, who, with batch filming, will not adjust the parameters for each image. Cases 1, 2, 5, and 6, in particular, showed that the demonstration of these sometimes subtle findings will depend on the use of nonroutine parameters. In addition, contrast between fluid levels might be enhanced by gradient-refocused imaging techniques, particularly in areas of hemorrhage.

The fluid levels composed of blood in different stages (cases 1, 2, and 4–6) were seen best on the T2-weighted sequence (Figs. 1E, 2B, 4A, 5B, and 6G). The more pronounced hypointensity of the dependent layer on the T2-weighted sequences compared with the T1 sequences resulted in superb contrast between the two components of the fluid level. The relatively blacker appearance of the dependent layer on T2-weighted images is believed to be related to the selective T2 shortening caused by intracellular paramagnetic substances such as intracellular deoxyhemoglobin or intracellular methemoglobin [1, 2].

Lastly, imaging in the prone position in case 1 (Fig. 1D) was extremely helpful in defining a solid nodule that was not clearly seen in the supine position. The relatively high signal intensity

of the nodule on the T1-weighted sequence made its visualization difficult against the high signal intensity of the surrounding free methemoglobin. In the prone position, however, the solid nodule remained fixed while the component fluid layers swapped positions. This enabled the nodule to be clearly seen against the surrounding layer of low signal intensity.

Discussion

MR Characteristics in Reported Cases

The MR signal characteristics in our six patients were helpful in identifying the contents of the fluid levels. Similar signal characteristics were seen in cases 1, 2, 4, and 5 (Figs. 1, 2, 4, and 5). In these cases the nondependent layers had high signal intensities on T1- and T2-weighted sequences. The dependent layers were hyperintense relative to brain on T1-weighted sequences (although less hyperintense than the nondependent layer) and became hypointense on T2-weighted sequences (Figs. 1C, 1E, 2B, 4A, and 5B). These signal characteristics were consistent with those described for various phases of subacute blood, as described in depth by other authors [1–6]. Subacute blood in the dilute methemoglobin phase has been shown to have high signal intensity on all pulse sequences. Intracellular methemoglobin has been described as having high signal on T1 sequences and low signal on T2 sequences, while intracellular deoxyhemoglobin appears hypointense to isointense on T1 sequences and hypointense on T2 sequences. However, as the hematoma evolves, intermediate stages are found containing both intracellular deoxyhemoglobin and intracellular methemoglobin, which may be variably hyperintense on the T1 images. Blood, as predicted, was demonstrated in all these cystic lesions,
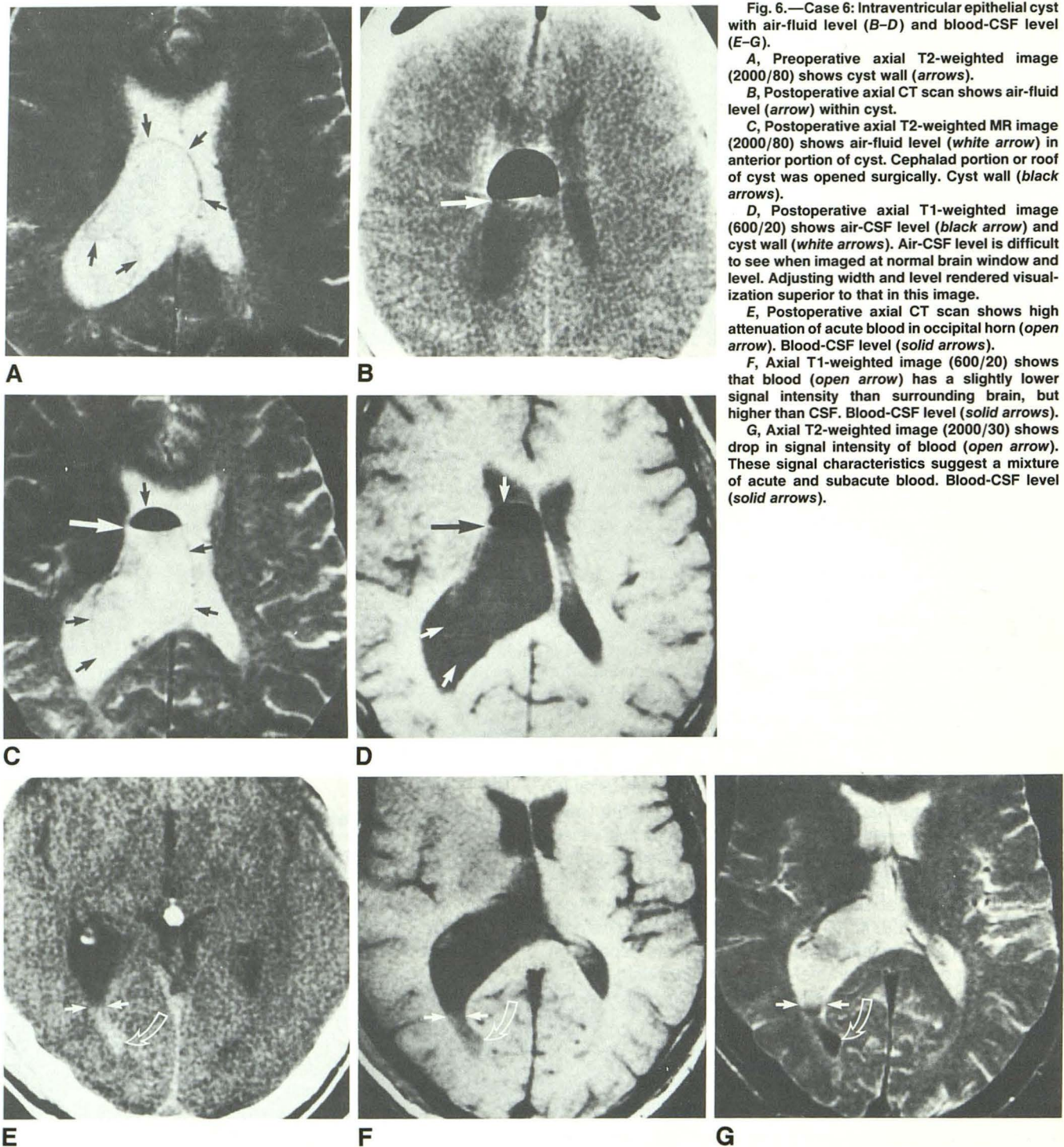
A

B

C

D

E

F

G

Fig. 6.—Case 6: Intraventricular epithelial cyst with air-fluid level (*B–D*) and blood-CSF level (*E–G*).

A, Preoperative axial T2-weighted image (2000/80) shows cyst wall (*arrows*).

B, Postoperative axial CT scan shows air-fluid level (*arrow*) within cyst.

C, Postoperative axial T2-weighted MR image (2000/80) shows air-fluid level (*white arrow*) in anterior portion of cyst. Cephalad portion or roof of cyst was opened surgically. Cyst wall (*black arrows*).

D, Postoperative axial T1-weighted image (600/20) shows air-CSF level (*black arrow*) and cyst wall (*white arrows*). Air-CSF level is difficult to see when imaged at normal brain window and level. Adjusting width and level rendered visualization superior to that in this image.

E, Postoperative axial CT scan shows high attenuation of acute blood in occipital horn (*open arrow*). Blood-CSF level (*solid arrows*).

F, Axial T1-weighted image (600/20) shows that blood (*open arrow*) has a slightly lower signal intensity than surrounding brain, but higher than CSF. Blood-CSF level (*solid arrows*).

G, Axial T2-weighted image (2000/30) shows drop in signal intensity of blood (*open arrow*). These signal characteristics suggest a mixture of acute and subacute blood. Blood-CSF level (*solid arrows*).

except in case 5 (recurrent craniopharyngioma). In case 5, where the patient refused repeat surgery, the presence of blood was inferred by its appearance on CT. In case 6 (intraventricular blood) the blood had slightly different signal characteristics. On the T1-weighted sequence, the blood had a slightly lower signal intensity than brain parenchyma, and on the T2-weighted sequence it dropped even further (Figs. 6F and 6G). This was consistent with blood in a more acute

phase (intracellular deoxyhemoglobin), the presence of which was readily explained by surgery the previous day. The signal intensity on the T1-weighted sequence being higher than that of CSF suggests a mixture with some subacute blood.

The appearance in cases 3 and 6 (air-fluid level), in which there was no blood, was completely different. In case 3 (cystic schwannoma), the nondependent layer had a low signal intensity on the T1-weighted sequence that was slightly higher in

intensity than CSF (Fig. 3B). On the T2-weighted sequence, the signal flipped to an intensity that was higher than that of CSF (Fig. 3C). These signal characteristics were typical of those described for nonhemorrhagic proteinaceous cysts [7], and at surgery a cystic schwanomma with proteinaceous fluid was encountered. No blood or hemosiderin was demonstrated at pathology. The dependent layer had a signal intensity that was similar to that of surrounding brain on both the T1- and T2-weighted sequences (Figs. 3B and 3C). It was not studied separately at pathology but was considered radiographically to represent necrotic debris. In case 6, an air-CSF level was present within an intraventricular epithelial cyst (Figs. 6A–6D). The nondependent air layer naturally had a signal void on all sequences, while the CSF layer demonstrated the usual characteristics of CSF.

Classification of Fluid Levels

Although MR signal characteristics are helpful in identifying the contents of the fluid levels, their formation is actually related to density differences within the layers. Fluid levels occur when two or more immiscible substances of unequal density coexist. In the human body we commonly encounter four "substances" with different densities: water, air, fat, and solids. The fluid levels we confront most frequently can therefore be classified into three groups: air-fluid, fat-fluid, and fluid-solid (precipitate) (Fig. 7).

Fluid-precipitate level.—Every patient in our series is included in the fluid-precipitate category. In the cystic schwannoma (case 3), the precipitate layer was composed of necrotic debris that settled to the bottom of the proteinaceous cyst, a finding that has been reported also in a cystic glioma [8]. In the fluid levels that contained blood in various stages of evolution, the precipitate layer was composed of cellular blood elements (cases 1, 2, 4, 5, and 6). Cohen et al. [9] have been able to demonstrate this phenomenon in vitro. They showed that both serum and plasma assume a nondependent position and have a high signal intensity of T1- and T2-weighted

images. RBCs assume a dependent position and have a low signal intensity on T2-weighted images. Therefore, while various stages of methemoglobin and deoxyhemoglobin are responsible for the signal characteristics, the physical formation of the fluid level is due to settling of the relatively denser cellular components. Other fluid-precipitate levels might also be seen in cerebral abscesses when inflammatory cells layer or in calcified cystic lesions when calcified products settle to the bottom.

Air-fluid level.—The MR appearance of an air-fluid level is nicely illustrated by case 6. The nondependent air layer should always have a signal void, while the dependent fluid layer could vary in signal intensity according to the amount of fat, protein, or blood within the fluid (Fig. 7).

An air-fluid level containing subacute blood might even have three layers: a nondependent air layer, a dependent layer containing intracellular methemoglobin or intracellular deoxyhemoglobin, and, in between, a layer containing free methemoglobin or free deoxyhemoglobin (Fig. 7). The air and free methemoglobin would have a signal void and a high signal intensity, respectively, on both the T1- and T2-weighted sequences, while the intracellular methemoglobin or intracellular deoxyhemoglobin would become markedly hypointense on the T2-weighted sequence. This would account for the appearance demonstrated in Figure 7.

Fat-fluid level.—None of our patients had intracranial fat-fluid levels on MR; however, they have been seen on CT in epidermoid tumors in the brain [10], ventricles [11], and subarachnoid spaces [11]. On MR we would expect a pure fat-fluid level to have a nondependent fatty layer characterized by high signal intensity on the T1-weighted sequence with a slight loss of signal intensity on the T2-weighted sequence. This is due to the relatively short T1 and T2 relaxation times of fat [12]. It is important to keep in mind, however, that the predicted appearance of the fatty layer may not always conform to this model [13]. With high-field-strength magnets we would also expect a chemical-shift artifact to occur between the lipid and aqueous interface in the frequency-encoding direction. On a multiecho axial scan the anterior aspect of the fatty component would have a rim of low signal (signal gap) while the posterior aspect would be expected to have a rim of high signal (signal overlap).

The dependent fluid layer in a fat-fluid level, as with CSF, would be expected to have a low signal intensity on the T1-weighted sequence and a high signal intensity on the T2-weighted sequence (Fig. 7). This is due to the long T1 and T2 relaxation times of relatively pure fluids [3, 7, 12]. Again, one must also keep in mind that not all fluids are in a relatively pure state like CSF. An increase in the protein content of a fluid shortens its T1 and T2 relaxation times [3, 7]. Under these conditions the fluid layer on the T1 sequence may have a signal intensity higher than CSF has, but usually lower than that of the surrounding brain parenchyma. At TRs used in routine T2-weighted imaging sequences, the signal intensity of a fluid with a high protein content may become brighter than CSF. This results from the relatively greater contribution of T1 shortening on signal intensity at routine imaging parameters [7]. Therefore, we can see that the predicted MR appearance of a fat-fluid level may vary, particularly in the
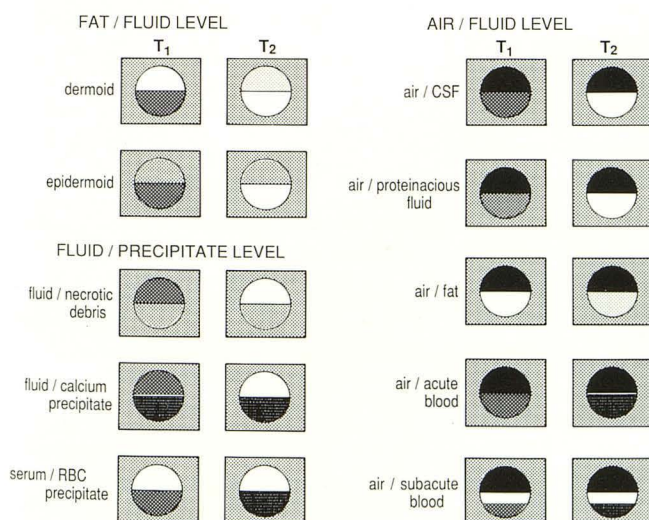

FAT / FLUID LEVEL

dermoid

epidermoid

FLUID / PRECIPITATE LEVEL

fluid / necrotic debris

fluid / calcium precipitate

serum / RBC precipitate

AIR / FLUID LEVEL

air / CSF

air / proteinacious fluid

air / fat

air / acute blood

air / subacute blood

Fig. 7.—MR appearances of fluid levels.

case of an epidermoid tumor. Dermoid tumors seem to behave more like pure fat-fluid levels (Fig. 7) [14].

Conclusions

We have described the MR characteristics of fluid levels and have classified fluid levels into three main groups: fat-fluid, air-fluid, and fluid-precipitate. It is important to remember, however, that the MR appearance of a specific lesion may vary according to the exact contents of the fluid level. For example, the fluid layers of two cystic lesions with the same pathologic diagnosis may appear different if the protein, fat, or blood contents of the fluid are different. It also seems clear, from this limited series, that MR is superior to CT in imaging fluid levels, and that analysis of MR signal characteristics can be most helpful in attempting to identify the contents of the fluid layers.

ACKNOWLEDGMENTS

REFERENCES

1. Gomori JM, Grossman RI, Goldberg HI, Zimmerman RA, Bilaniuk LT. Intracranial hematomas: imaging by high field MR. *Radiology* **1985**; 157:87–93

2. Gomori JM, Grossman RI, Hackney DB, Goldberg HI, Zimmerman RA, Bilaziuk LT. Variable appearance of subacute intracranial hematomas on high-field spin-echo MR. *AJNR* **1987**;8:1019–1026, *AJR* **1988**;150: 171–178

3. Bradley WG. Pathophysiologic correlates of signal alterations. In: Brant-Zawadzki M, Norman D, eds. *Magnetic resonance imaging of the central nervous system.* New York: Raven, **1986**:23–42

4. Norman D. Vascular disease: hemorrhage. In: Brant-Zawadzki M, Norman D, eds. *Magnetic resonance imaging of the central nervous system.* New York: Raven, **1986**:209–220

5. Gomori JM, Grossman RI. Mechanisms responsible for the MR appearance and evolution of intracranial hemorrhage. *RadioGraphics* **1988**;8:427–440

6. Grossman RI, Gomori JM, Goldberg HI, et al. MR imaging of hemorrhagic conditions of the head and neck. *RadioGraphics* **1988**;8:441–454

7. Kjos BO, Brant-Zawadzki M, Kucharczyk W, Kelly WM, Norman D, Newton TH. Cystic intracranial lesions: magnetic resonance imaging. *Radiology* **1985**;155:363–369

8. Brant-Zawadzki M, Kelly W. Brain tumors. In: Brant-Zawadzki M, Norman D, eds. *Magnetic resonance imaging of the central nervous system.* New York: Raven, **1986**:151–185

9. Cohen MD, McGuire W, Cory DA, Smith JA. MR appearance of blood and blood products: an in vitro study. *AJR* **1986**;146:1293–1297

10. Cornell SH, Graf CJ, Dolan KD. Fat-fluid level in intracranial epidermoid cyst. *AJR* **1977**;128:502–503

11. Laster WD, Moody DM, Marshall RE. Epidermoid tumors with intraventricular and subarachnoid fat: report of two cases. *AJR* **1977**;128:504–507

12. Pavlicek W, Modic M, Weinstein M. Pulse sequence and significance. *RadioGraphics* **1984**;4:49–65

13. Vion-Dury J, Vincentelli F, Jiddave M, et al. MR imaging of epidermoid cysts. *Neuroradiology* **1987**;29:333–338

14. Batnitzky S, Price HI, Gresick RJ, McMillan JH, Danziger A, Rosenthal S. Intracranial pearly tumors: radiologic evaluation, past and present. *Radiology* **1987**;165P[suppl]:401–402